https://doi.org/10.20965/ijat.2020.p0534

Paper:

Processing with Application of High-Power Semiconductor Laser – Theoretical Analysis of Heat Source and Application to Surface Processing –

Takeji Arai†

Research and Development Initiative, Chuo University
1-13-27 Kasuga, Bunkyo-ku, Tokyo 112-8551, Japan
†Corresponding author, E-mail: tarai@tamacc.chuo-u.ac.jp
[Received January 9, 2020; accepted March 24, 2020]

Since the semiconductor laser has a high conversion efficiency, it has many expectations for effective application. There are increasing application trials of processing at actual factories and jobsites. Moreover, it can currently be used as a heat source to directly conduct processing. This is called direct-diode laser (DDL). However, since there is almost no information regarding the DDL structure and beam mode, there are no scientific documents for the theoretical treatment of this heat source. This is considered to have interfered with the broad application for development. This research establishes the theoretical analysis of the semiconductor heat source for material processing, and we attempted to employ a simulation for processing. To verify the established theory, surface hardening and welding processing were performed as typical processing.

Keywords: laser processing, semiconductor laser, direct-diode laser, heat treatment

1. Introduction

Theoretical analysis studies on laser hardening of metal surfaces have been reported at conferences since 1975. Initially, most lasers were carbon dioxide gas lasers with either a circular heat source or a Gaussian-distribution heat source as calculation model of the heat source [1–4]. In the 2000s, high-power, solid-state lasers attracted global attention as processing lasers. Such lasers include fiber, disk, and semiconductor lasers. In particular, the semiconductor laser power was sufficiently high that the laser could be used directly for processing. In addition, the semiconductor laser is known for its high conversion efficiency from electricity to laser and is currently used in a variety of industries. Moreover, there are technological reports and academic papers concerning promising prospects and possible industrial applications of the semiconductor laser [5–9]. However, detailed information on novel high-power semiconductor lasers have not been fully disclosed. In addition, since the energy intensity of the high-power, semiconductor laser heat source has a characteristic distribution, few studies have investigated the semiconductor laser heat source theoretically. Therefore, most papers and reports on direct-processing semiconductor laser focus on the results of experimental processing [10–14]. This situation could hinder the application and future development of various processing technologies using the semiconductor laser.

In this study, we measured the energy-intensity distribution of the semiconductor laser and used the obtained distribution to create a model, which was then used for the numerical analysis of processing. Moreover, for comparison of the analytical results with experiments, we performed, under the same conditions, surface hardening and bead-on-plate experiments in which the heat source moved over the material surface at a constant speed. After a comprehensive comparison, the processing depth of the surface hardening was found to be larger using the semiconductor laser than the CO_2 laser. Furthermore, the simulation result indicated that new applications could be made by changing the parallel layout or the interval. Therefore, it was found that the semiconductor laser could be useful as a heat source for surface processing such as hardening.

2. Semiconductor and Direct-Processing Lasers

2.1. High-Power Direct-Diode Laser (Direct-Processing Semiconductor Laser)

Initially, semiconductor laser devices (laser diodes) had a power of only approximately 5 W and were used to replace the lamps of lamp-pumped YAG lasers. Then, higher powers were achieved through technological development. Several semiconductor chips were aligned in an array (bar array) to enhance the power, and then several LD arrays were stacked to produce substantially higher power than the two-dimensional array. With this high power, the semiconductor laser started to be used directly for processing. This kind of semiconductor laser is called the direct-processing semiconductor laser (DDL: direct-

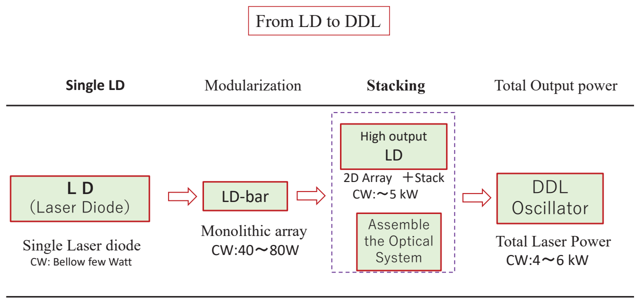

Fig. 1. Procedures for achieving high output of direct-diode laser.

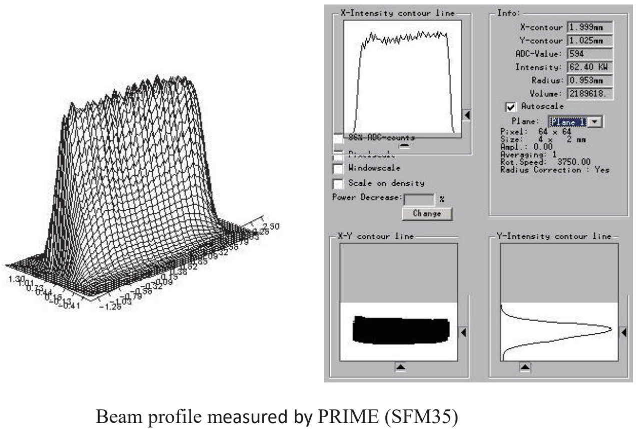

Fig. 2. High-power laser beam intensity distribution of direct-diode laser.

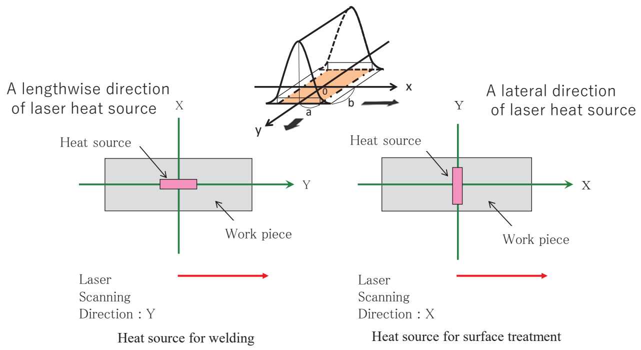

Fig. 3. Definition of lengthwise direction and lateral direction of laser heat source during processing.

diode laser).

In comparison with other lasers, the semiconductor laser is known to have extremely high efficiency, approximately 50%, in the conversion of given electricity to laser (electricity-optical conversion efficiency). Further advantages include long life and compact size. In the early stage, the power per LD bar was 20–40 W. However, owing to technological improvement in light concentration and heat radiation design, the current minimum power of the single-bar type semiconductor (laser diode) is approximately 300 W. Array technology or layer technology enhanced the semiconductor laser power further to approximately 4–6 kW. Moreover, the polarization multiplexing technique of the laser beam realized the power of up to 25 kW. An increasing number of processing-device manufacturers have employed direct-processing semiconductor lasers since their conversion efficiency is extremely high. **Fig. 1** shows the recent development move toward high-output lasers. As a result of the development of high-power semiconductor lasers for industrial applications, the laser can now be used for various processing works.

2.2. Energy-Intensity Distribution of Semiconductor Laser

The energy intensity of a high-power semiconductor laser heat source has a characteristic distribution; the intensity distribution needs to be clarified. Therefore, we measured and visualized the energy-intensity distribution of a laser beam using laser beam profiler (FocusMonitor FM35, PRIMES) and obtained the result shown in **Fig. 2**. From the measurement results, one can see that both individual LDs and the single DDL composed of overlapped LDs have almost identical heat source distributions, namely a rectangular distribution on the bottom and a Gaussian distribution on the side cross section. This indicates that the heat source shape of the material changes with the movement direction of the heat source because of the rectangular bottom shape, as shown in **Fig. 3**. Therefore, the type of processing suitable for the industrial application depends on the movement direction. If the heat source moves in the x-direction, i.e., the direction perpendicular to the wider edge of the heat source, the processing is suitable for surface processing such as hardening. If the heat source moves in the y-direction, i.e., the direction perpendicular to the narrower edge of the heat source, the processing is suitable for welding. For this reason, we need to derive theoretical equations of two kinds of heat-source models for different movement directions of the heat source, namely the x- and y-directions.

3. Theoretical Analysis of Semiconductor Laser as a Heat Source

The heat source shape measurements show that a semiconductor laser heat source could be approximated with a rectangular-Gaussian heat source. According to this mathematical model, the heat conduction state changes depending on the movement direction (running direction) of the heat source. Therefore, a mathematical analysis needs to be performed for each direction. The analysis performed is shown as follow.

3.1. Movement in the Longitudinal Direction (y-direction)

When a heat source with a certain intensity is placed above a semi-infinite material, the temperature rise at a point (x, y, z) in the material whose surface is heated is expressed in general by the following formula based on the assumption that there is no heat loss from the surface [15].

$$\theta=\frac{\alpha}{4K(\pi\alpha)^{\frac{3}{2}}}\int_{-\infty}^{\infty}\int_{-\infty}^{\infty}\int_{0}^{\infty}\frac{w(x',y')}{\sqrt{t^3}}\times e^{-\frac{(x-x')^2+(y-y')^2+z^2}{4\alpha t}}\,dt\,dx'dy'.$$

Here, K is the thermal conductivity [W/cm·K] or [kcal/m·h·°C], α the thermal diffusivity [cm^2/s], and t the time [s].

In addition, if the heat source above the surface has an energy distribution $w(x',y')$, as shown in **Fig. 3**, the x- and y-direction lengths of the rectangle at the bottom of the heat source are denoted by $2a$ and $2b$, respectively. The energy distribution $w(x',y')$ for a rectangular-Gaussian distribution heat source is given by the following equation with W representing the laser output [W]. In this case, the heat source is narrow.

$$w(x',y')=\frac{W}{2ab\sqrt{\pi}}e^{-\frac{x^2}{a^2}}F(y)$$

$$F(y)=\begin{cases}1, & |y|\le b,\\ 0, & |y|>b.\end{cases}$$

If the heat source moves in the y-direction at a speed v, this equation becomes the following, with A representing the laser-beam absorption rate.

$$\theta=\frac{A\alpha}{4K\sqrt{(\pi\alpha)^3}}\int_{-\infty}^{\infty}\int_{-\infty}^{\infty}\int_{0}^{\infty}\frac{\frac{W}{2ab\sqrt{\pi}}}{\sqrt{t^3}}e^{-\frac{x^2}{a^2}}\times e^{-\frac{(x-x')^2+(y-y'+vt)^2+z^2}{4\alpha t}}\,dt\,dx'dy'. \qquad (1)$$

Using the following symbols,

$$I_x=\int_{-\infty}^{\infty}e^{-\frac{x^2}{a^2}-\frac{(x-x')^2}{4\alpha t}}\,dx',$$

$$I_y=\int_{-b}^{+b}e^{-\frac{(y-y'+vt)^2}{4\alpha t}}\,dy',$$

$$I_z=\int_{0}^{\infty}\frac{e^{-\frac{z^2}{4\alpha t}}}{\sqrt{t^3}}\,dt,$$

Eq. (1) is rewritten as follows.

$$\theta=\frac{A\alpha\cdot\frac{W}{2ab\sqrt{\pi}}}{4K\sqrt{(\pi\alpha)^3}}\int_{0}^{\infty}\frac{e^{-\frac{z^2}{4\alpha t}}}{\sqrt{t^3}}\,dt\int_{-\infty}^{\infty}e^{-\frac{x^2}{a^2}-\frac{(x-x')^2}{4\alpha t}}\,dx'\times\int_{-b}^{+b}e^{-\frac{(y-y'+vt)^2}{4\alpha t}}\,dy'.$$

Then, it becomes

$$\theta=\frac{AW}{8Kab\pi^2\sqrt{\alpha}}\int_{0}^{\infty}\frac{e^{-\frac{z^2}{4\alpha t}}}{\sqrt{t^3}}\cdot I_x\cdot I_y\,dt, \qquad (2)$$

where

$$\begin{aligned}I_x&=\int_{-\infty}^{\infty}e^{-\frac{x^2}{a^2}-\frac{(x-x')^2}{4\alpha t}}\,dx'\\&=\int_{-\infty}^{\infty}e^{-\left(\frac{x'^2}{a^2}+\frac{x^2-2xx'+x'^2}{4\alpha t}\right)}\,dx'\\&=e^{-\frac{x^2}{4\alpha t}}\int_{-\infty}^{\infty}e^{-\left(\frac{1}{a^2}+\frac{1}{4\alpha t}\right)x'^2+\frac{x}{2\alpha t}x'}\,dx'\\&=e^{-\frac{x^2}{4\alpha t}}\int_{-\infty}^{\infty}e^{-\left(\frac{a^2+4\alpha t}{4a^2\alpha t}\right)x'^2+\left(\frac{x}{2\alpha t}\right)x'}\,dx'.\end{aligned}$$

In addition, if we use

$$A_x=\sqrt{\frac{a^2+4\alpha t}{4a^2\alpha t}},\quad B_x=\frac{ax}{2\sqrt{\alpha t\,(a^2+4\alpha t)}},$$

the preceding equation becomes

$$\begin{aligned}I_x&=e^{-\frac{x^2}{4\alpha t}}\int_{-\infty}^{\infty}e^{B_x{}^2-\left(\sqrt{\frac{a^2+4\alpha t}{4a^2\alpha t}}x'-B_x\right)^2}\\&=e^{B_x{}^2-\frac{x^2}{4\alpha t}}\int_{-\infty}^{\infty}e^{-\left(A_xx'-B_x\right)^2}\,dx',\end{aligned}$$

$$\int_{-\infty}^{\infty}e^{-u^2}\,du=2\int_{0}^{\infty}e^{-u^2}\,du=\sqrt{\pi}.$$

Now we set $A_xx'-B_x=u$ and obtain $dx'=(1/A_x)du$ and

$$I_x=e^{B_x{}^2-\frac{x^2}{4\alpha t}}\int_{-\infty}^{\infty}e^{-u^2}\frac{du}{A_x}=\frac{\sqrt{\pi}}{A_x}\cdot e^{B_x{}^2-\frac{x^2}{4\alpha t}}.$$

Since we have

$$B_x{}^2-\frac{x^2}{4\alpha t}=\frac{a^2x^2}{4\alpha t\,(a^2+4\alpha t)}-\frac{x^2}{4\alpha t}=-\frac{x^2}{a^2+4\alpha t},$$

the equation can be rewritten as follows.

$$I_x=\frac{\sqrt{\pi}}{A_x}\cdot e^{-\frac{x^2}{a^2+4\alpha t}}=\sqrt{\frac{4\pi a^2\alpha t}{a^2+4\alpha t}}\cdot e^{-\frac{x^2}{a^2+4\alpha t}}. \qquad (3)$$

To make the quantities dimensionless, we set

$$\frac{a}{r}=\Re,\quad\frac{rv}{4\alpha}=U,\quad 4\alpha t=r^2p^2,$$

where v is the speed and r the radius of the Gaussian heat source (defined in terms of $1/e^2$). Then, we obtain

$$dt=\frac{r^2}{2\alpha}\cdot p\,dp,\quad t=\frac{r^2}{4\alpha}\cdot p^2,$$

$$I_x=\frac{\sqrt{\pi}\Re rp}{\sqrt{\Re^2+p^2}}\cdot e^{-\frac{X^2}{\Re^2+p^2}}, \qquad (4)$$

and

$$I_y=\int_{-b}^{+b}e^{-\frac{(y-y'+vt)^2}{4\alpha t}}\,dy'.$$

Further, to make the quantities dimensionless, we set

$$4\alpha t=r^2p^2.$$

Then we obtain

$$I_y = \int_{-b}^{+b} e^{-\frac{\left[y-y'+v\left(\frac{r^2p^2}{4\alpha}\right)\right]^2}{r^2p^2}} dy'$$
$$= \int_{-b}^{+b} e^{-\frac{\left[\left\{y-y'+v\left(\frac{r^2p^2}{4\alpha}\right)\right\}/r\right]^2}{p^2}} dy'.$$

Moreover, if we set

$$\frac{y-y'+vt}{r} = Y', \quad dy' = -r\,dY$$
$$y' = +b: \quad Y' = \frac{y-b+vt}{r}$$
$$y' = -b: \quad Y' = \frac{y+b+vt}{r}$$

we have

$$I_y = \int_{\frac{y+b+vt}{r}}^{\frac{y-b+vt}{r}} e^{-\frac{Y'}{p^2}}\left(-r\,dY'\right) = r\int_{\frac{y-b+vt}{r}}^{\frac{y+b+vt}{r}} e^{-\left(\frac{Y'}{p^2}\right)^2} dY'.$$

If we also set

$$\frac{y}{r} = Y, \quad \frac{b}{r} = B, \quad \frac{Y'}{r} = \eta, \quad dY' = p\,d\eta,$$
$$Y' = \frac{y+b+vt}{r} = Y+B+Up^2,$$
$$\frac{vr}{4\alpha} = U, \quad \eta = \frac{Y+B+Up^2}{p},$$

we obtain

$$I_y = r\int_{\frac{Y-B+Up^2}{p}}^{\frac{Y+B+Up^2}{p}} e^{-\eta}\,p\,d\eta$$
$$= rp\cdot\frac{\sqrt{\pi}}{2}\left[erf\left(\frac{Y+B+Up^2}{p}\right) - erf\left(\frac{Y-B+Up^2}{p}\right)\right]. \quad \dots\dots (5)$$

If we set

$$4\alpha t = r^2p^2, \quad \frac{z^2}{r^2p^2} = \frac{{Z_0}^2}{p^2}, \quad \frac{z}{r} = Z_0,$$
$$t = \frac{r^2p^2}{4\alpha}, \quad dt = \frac{r^2}{2\alpha}\cdot p\,dp$$

we obtain

$$I_z = \int_0^{\infty} \frac{e^{-\frac{z^2}{r^2p^2}}}{\sqrt{t^3}} dt$$
$$= \int_0^{\infty} \frac{e^{-\frac{z^2}{4\alpha t}}}{\sqrt{\left(\frac{r^2p^2}{4\alpha}\right)^3}}\cdot\frac{r^2}{2\alpha}\cdot p\,dp,$$

and

$$I_z = \int_0^{\infty} \sqrt{\frac{(4\alpha)^3}{(r^2p^2)^3}}\cdot\frac{r^2}{2\alpha}\cdot e^{-\frac{{Z_0}^2}{p^2}}\,p\,dp$$
$$= \int_0^{\infty} \frac{4\sqrt{\alpha}}{rp^2}\cdot e^{-\frac{{Z_0}^2}{p^2}}\,dp. \quad \dots\dots\dots (6)$$

Inserting Eqs. (4)–(6) into Eq. (2), we have

$$\theta = \frac{AW}{8Kab\pi^2\sqrt{\alpha}}\int_0^{\infty} \frac{4\sqrt{\pi}}{\sqrt{t_3}}\cdot e^{-\frac{{Z_0}^2}{p^2}}\cdot\frac{\sqrt{\pi}\Re rp}{\sqrt{\Re^2+p^2}}$$
$$\times e^{-\frac{X^2}{\Re^2+p^2}}\cdot rp\cdot\frac{\sqrt{\pi}}{2}\left[erf\left(\frac{Y+B+Up^2}{p}\right) - erf\left(\frac{Y-B+Up^2}{p}\right)\right]dp$$
$$= \frac{AW}{4\pi Kb}\int_0^{\infty} \frac{e^{-\frac{x^2}{\Re^2+p^2}-\frac{{Z_0}^2}{p^2}}}{\sqrt{\Re^2+p^2}}\left[erf\left(\frac{Y+B+Up^2}{p}\right) - erf\left(\frac{Y-B+Up^2}{p}\right)\right]dp. \quad (7)$$

Thus, we obtained the temperature distribution of a stationary state with a heat source with a rectangular-Gaussian energy distribution, moving in the y-direction at speed v [13].

3.2. Movement in the Lateral Direction (x-direction)

Similarly, as shown in **Fig. 3**, the x- and y-direction lengths of the rectangle at the bottom of the heat source are denoted by $2a$ and the $2b$, respectively. Since the rectangular-Gaussian energy distribution with a heat source moving in the x-direction at a constant speed v is already given, the temperature distribution can be written as follows. In this case, the heat source width increases.

$$\theta = \frac{A\alpha}{4K\sqrt{(\pi\alpha)^3}}\int_{-\infty}^{\infty}\int_{-\infty}^{\infty}\int_0^{\infty} \frac{\frac{W}{2ab\sqrt{\pi}}F(y)}{\sqrt{t^3}}\cdot e^{-\frac{x^2}{a^2}}$$
$$\times e^{-\frac{(x-x'+vt)^2+(y-y')^2+z^2}{4\alpha t}}\,dt\,dx'dy'. \quad \dots\dots (8)$$

If we set

$$I_x = \int_{-\infty}^{\infty} e^{-\frac{x^2}{a^2}-\frac{(x-x'+vt)^2}{4\alpha t}}\,dx',$$
$$I_y = \int_{-b}^{+b} e^{-\frac{(y-y')^2}{4\alpha t}}\,dy',$$
$$I_z = \int_0^{\infty} \frac{e^{-\frac{z^2}{4\alpha t}}}{\sqrt{t^3}}\,dt,$$

Eq. (8) becomes

$$\theta = \frac{AW}{8Kab\pi^2\sqrt{\alpha}}\int_0^{\infty} \frac{e^{-\frac{z^2}{4\alpha t}}}{\sqrt{t^3}}\,dt\int_{-\infty}^{\infty} I_x\cdot I_y\,dt. \quad . \quad (9)$$

To make the formula dimensionless, we have

$$
\begin{aligned}
I_x &= \int_{-\infty}^{\infty} e^{-\frac{x^2}{a^2}-\frac{(x-x'+vt)^2}{4\alpha t}}\,dx' \\
&= \sqrt{\frac{\pi 4a^2\alpha t}{a^2+4\alpha t}}\cdot e^{-\frac{(x-vt)^2}{a^2+4\alpha t}} \\
&= \frac{\sqrt{\pi}\Re rp}{\sqrt{\Re^2+p^2}}\cdot e^{-\frac{\left(X+Up^2\right)^2}{\Re^2+p^2}} \quad . \ . \ . \ . \ . \ . \ . \ . \ (10)
\end{aligned}
$$

$$
\begin{aligned}
I_y &= \int_{-b}^{+b} e^{-\frac{(y-y')^2}{4\alpha t}}\,dy' \\
&= rp\cdot\frac{\sqrt{\pi}}{2}\left[erf\left(\frac{Y+B}{p}\right)-erf\left(\frac{Y-B}{p}\right)\right], \quad (11)
\end{aligned}
$$

where

$$
\begin{aligned}
&4\alpha t = r^2p^2, \quad dt = \frac{2r^2}{4\alpha}\cdot p\,dp, \\
&\frac{x}{r} = X, \quad \frac{y}{r} = Y, \quad \frac{z}{r} = Z_0, \\
&\frac{a}{r} = \Re, \quad \frac{b}{r} = B, \quad \frac{rv}{4\alpha} = U.
\end{aligned}
$$

$$
\begin{aligned}
\theta = \frac{AW}{8Kab\pi^2\sqrt{\alpha}}\int_0^{\infty}\frac{e^{-\frac{z^2}{r^2p^2}}}{\sqrt{\left(\frac{r^2p^2}{4\alpha}\right)^3}} \\
\times\frac{\sqrt{\pi}\Re rp}{\sqrt{\Re^2+p^2}}\cdot e^{-\frac{\left(X+Up^2\right)^2}{\Re^2+p^2}}\cdot rp\cdot\frac{\sqrt{\pi}}{2}\left[erf\left(\frac{Y+B}{p}\right)\right. \\
\left.-erf\left(\frac{Y-B}{p}\right)\right]\frac{r^2}{2\alpha}\cdot p\,dp. \quad (12)
\end{aligned}
$$

Therefore, we have

$$
\begin{aligned}
\theta = \frac{AW}{4\pi Kb}\int_0^{\infty}\frac{e^{-\frac{\left(X+Up^2\right)^2}{\Re^2+p^2}-\frac{Z_0{}^2}{p^2}}}{\sqrt{\Re^2+p^2}}\left[erf\left(\frac{Y+B}{p}\right)\right. \\
\left.-erf\left(\frac{Y-B}{p}\right)\right]dp. \quad . \quad (13)
\end{aligned}
$$

Thus, we obtained the temperature distribution of a stationary state with a heat source with a rectangular-Gaussian energy distribution, moving in the x-direction at a speed v [13].

These equations express the temperature distribution of the surface and inside of a material when a moving laser heat source is applied to the surface. Most cases where the processing does not involve melting the metal, such as hardening, can be expressed by these equations. However, if the processing involves surface melting or if melting causes the metal to thermal expand or molten-metal flow, simulations must be performed to obtain accurate results.

4. Analytical Solution and Simulation Results

4.1. Numerical Calculation with Analytical Solution

The high-power semiconductor laser (DDL) uses multiple stacked heat sources. There are two methods of use. One is to overlap them for use as a single heat source, and the other is to align them at constant intervals for use as multiple heat sources and to heat the material successively. We call the former "synthesized heat source" and the latter "parallel heat sources aligned successively." In the following sections, we show the calculation results and simulation results for comparison.

4.2. Simulation with Three-Dimensional Nonstationary Elastoplasticity Analysis

This simulation, newly improved by the authors for high-power laser processing of metals, is a thermal analysis software using the finite element method. In this simulation method, the laser heat source is replaced with a heat flux which is then converted to a heat quantity, and the temperature is calculated by considering the beam-absorption rate and the thermal absorption property of the material. The temperature field can be calculated using the heat conduction equation with irradiation and convection, considering the contact heat transfer. Thus, the simulation is a three-dimensional, nonstationary, elastoplasticity analysis software that calculates the elastoplastic stress distortion from the temperature for a given heat.

Material thermally deforms at high temperatures if it continuously receives laser-beam radiation from a heat source moving at a constant speed. The deformation state can be calculated by the three-dimensional, nonstationary, elastoplasticity analysis. In this calculation, radiation and convection are taken into account for contact heat transfer at the nodal points of the elements. The temperature dependence is considered to calculate the physical properties; additionally, the latent heat of fusion is taken into account for molten state. This allows a time-series calculation of expansion and deformation due to metal melting in the process of laser processing, as well as the calculation of the final residual stress and deformed state. In the case of no deformation, only the temperature distribution due to the heat conduction is shown. **Fig. 4** shows the calculation flow.

The temperature-dependent thermal constants such as thermal conductivity, thermal diffusivity, and specific heat and the absorption rate which changes with the speed of the moving heat sources, used in the calculation are shown in Appendixes A and B.

(i) Synthesized heat source

This is a method to synthesize a heat source by overlapping heat sources of several stacks that emit light. As a result, the heat sources can be expressed as a single heat source. In this case, although the total power increases, the derived equations can be used for calculation.

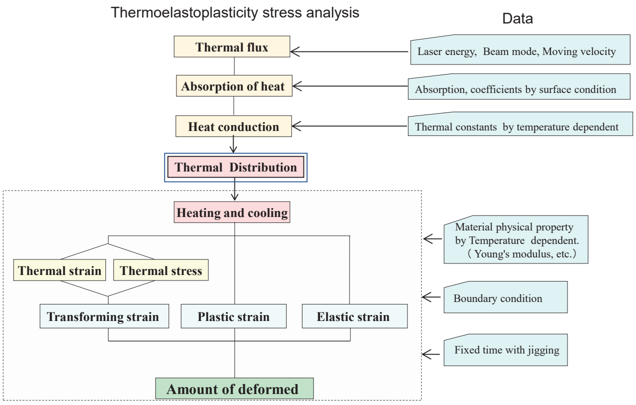

Fig. 4. Flow chart of simulation.

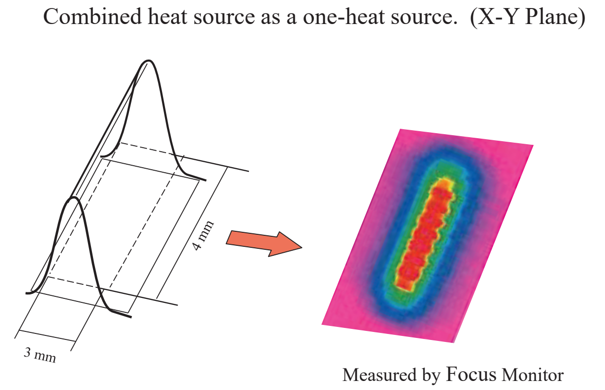

Fig. 5. Measurement of combined source area as a single heat source during x-direction movement.

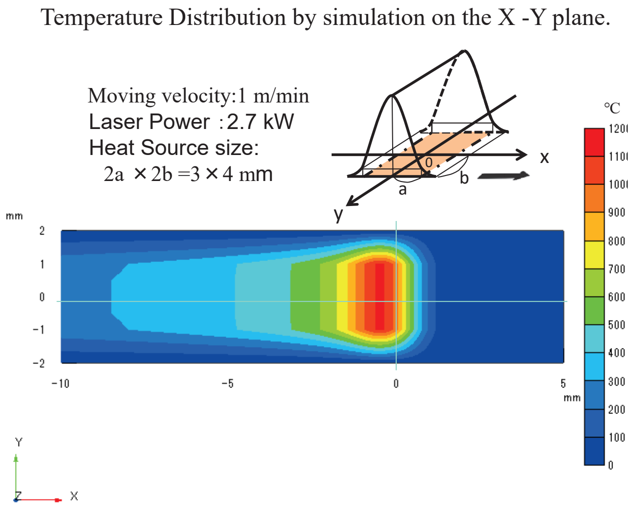

Fig. 6. Simulation results of combined heat source as a single heat source during x-direction movement.

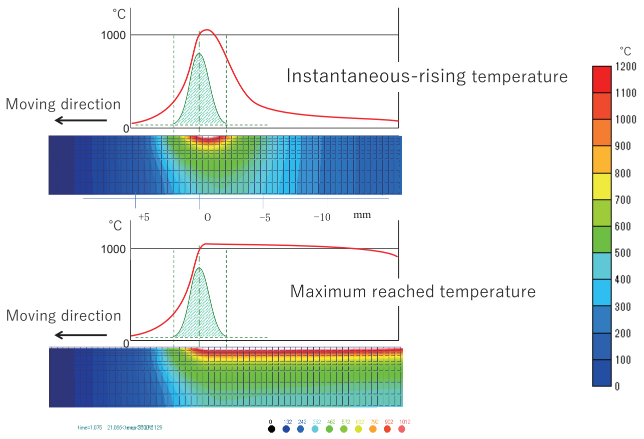

Fig. 7. Simulation results of temperature distribution on X-Z plane as a single heat source.

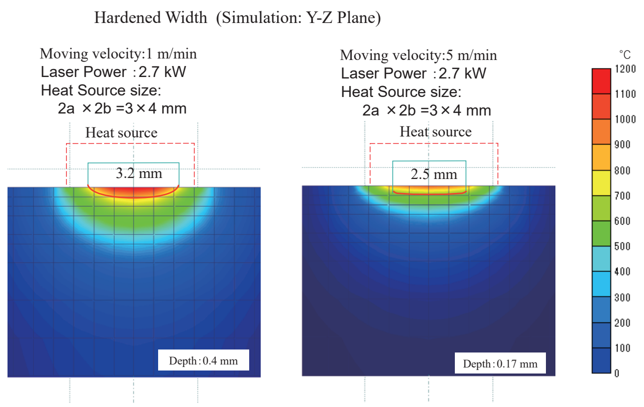

Fig. 8. Simulation results of temperature distribution for the laser heat source moving in the x-direction.

The simulation result of the X-Y plane with a single synthesized heat source moving in the x-direction is shown in **Fig. 5**. The heat sources are overlapped at a single point, forming a single rectangular heat source. **Fig. 6** shows the temperature distribution on the X-Y plane, with a synthesized heat source of size of 3 mm × 4 mm and power 2.7 kW that moves along the material surface at a speed of 1 m/min. **Fig. 7** shows the simulation results of the instantaneous temperature reached on the X-Z plane and the change in the maximum temperature with the motion of the heat source. To harden the metal, the material temperature needs to be higher than the transformation point A_1 and lower than the melting point. After laser radiation, the material naturally cools and changes to a hardened structure. In general, the transformation point A_1 of carbon steel is 727°C or higher when hardened. In contrast, high-speed heating/cooling processing such as laser hardening processing hardens material at temperatures 100°C higher than this [1, 2].

Figure 8 shows the simulation result of the temperature distribution on the Y-Z plane under the same condition. For the speed of 1 m/min, the hardened width and depth are 3.2 mm and 0.4 mm, respectively. For the speed of 5 m/min, the hardened width and depth are 2.5 mm and 0.174 mm, respectively. Here, the hardened width is the maximum width of the surface area hardened by the structural change due to hardening processing with laser radiation. The width is measured by observing the metal structure after the hardening processing. The hardened depth

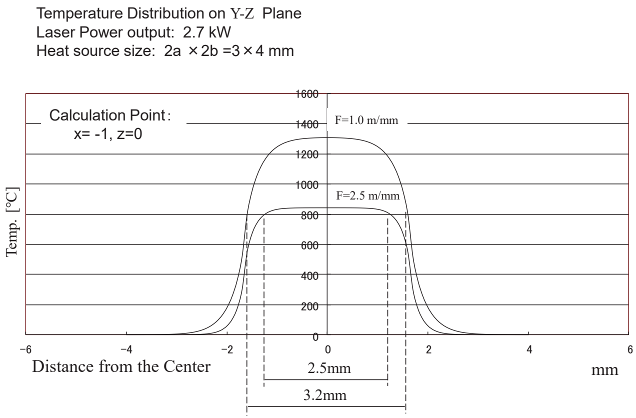

Fig. 9. Theoretical calculation results of temperature distribution and hardening width with x-direction movement of the laser heat source.

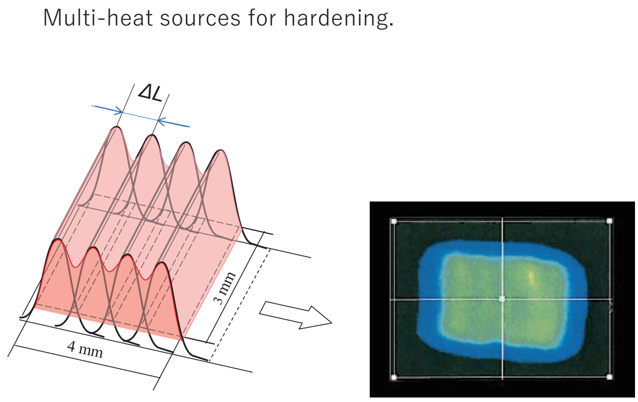

Fig. 10. Projection-chart image of the heat source on the screen of the CCD camera.

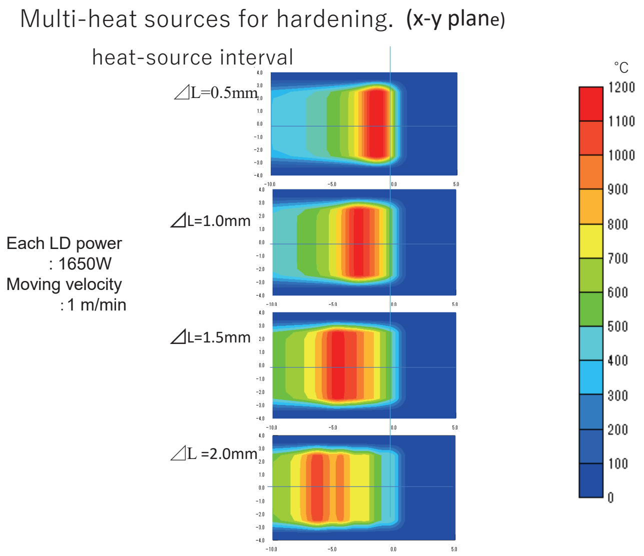

Fig. 11. Simulation results of the surface temperature for varying distance of each LD heat source (x-direction movement).

is the maximum depth of the hardened circular arc from the surface. In addition, the area with structural change is called the hardened area. These dimensions are measured by observing the cross-sectional structure of the metal. The measured width and depth are indicated in **Figs. 16** and **17** (Section 5.2.1).

As an example of calculation using Eq. (13) under this condition, **Fig. 9** shows the temperature distribution on the cross-section (Y-Z plane) with a power of 2.7 kW and speeds of 1 and 2.5 m/min. The calculation point is set to $x = -1$ because the temperature reaches a maximum at a point behind the origin. Since the heat source moves in the x-direction, the temperature distribution is relatively wide in the lateral direction.

The center rises slightly when the speed is low and tends to be flat when the speed is high. In the figure of the theoretically calculated temperature distribution, the lines represent width of the hardened area obtained from the simulations.

(ii) Successively aligned heat sources

Here, we show the method of using multiple heat sources aligned successively in parallel. In this case, the LD heat sources are aligned successively on the material surface with an interval of several millimeters; the interval largely affects the surface temperature during hardening or other processing. This configuration can be used in actual equipment if the appropriate optical alignment is realized; however, we show the simulation results here. **Fig. 10** shows the conceptual diagram and the projection of a light image of four successively aligned heat sources on a plane screen taken by a CCD camera. We see that a wide area of the surface is heated.

Now, we show a calculation example of multiple heat sources successively aligned. In the calculation, we assume four stacked heat sources and study how a change in the heat source configuration affects the temperature distribution on the heated surface. **Fig. 11** shows the temperature distribution on the material surface for different heat-source intervals of $x = 1.0$, 1.5, and 2.0 mm. A change in the interval of the four heat sources that successively heat the surface affects the heating time and temperature, and hence the hardened area. The figure shows the temperature distributions of the four LD lasers at different constant intervals. With a wider interval, the heated area is larger, but the maximum temperature is lower. Moreover, it is known that when the maximum temperature decreases, an intermediate structure could form in the boundary between the hardened area and the original material [3]. **Fig. 12** gives details of the temperature distribution inside the material with a heat-source interval of 2 mm and at an identical power. The temperature is higher at points closer to the surface and the isothermal lines become closer to each other at deeper points.

Now, we discuss a calculation example. **Fig. 13** shows the temperature distribution on the X-Y plane for different intervals, with the four LD heat sources moving in the x-direction with constant power. The temperature reaches a maximum at a point slightly behind the center of the heat

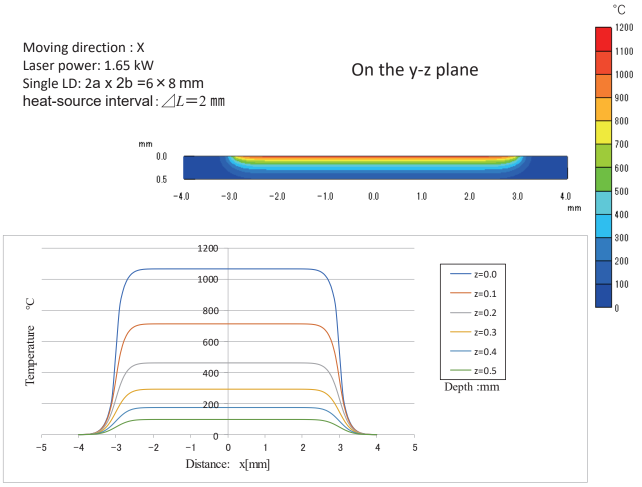

Fig. 12. Temperature distribution in the depth direction using four LDs for the case of $\Delta L = 2$ mm.

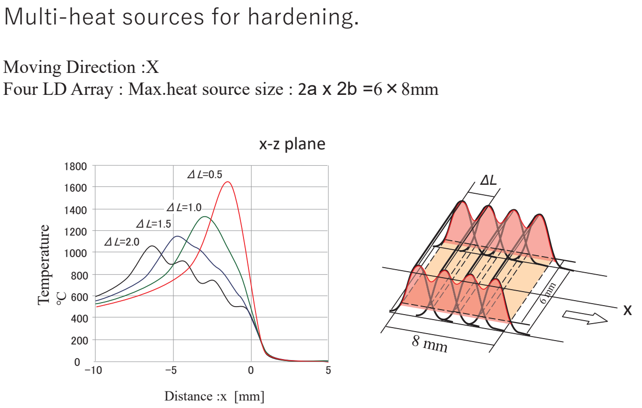

Fig. 13. Calculation results of the surface temperature for varying distances between the LD heat sources.

sources in the movement direction. With small intervals of the LD heat sources, the maximum temperature is high and the temperature distribution appears identical to that of the single heat source. However, with large intervals of the LD heat sources, the maximum temperature is low and the temperature distribution indicates multiple peaks corresponding to the heat sources.

Figure 14 shows that a uniform maximum temperature is maintained in the heated area by appropriate control of the output ratio of the four heat sources. This means that one can apply a sufficiently high hardening temperature to a material for a long period of time. For conventional laser hardening of a large area with a narrow heat source, one needs to gradually move the single, narrow heat source in the lateral direction so that the ends of each heated line overlap with those of the previous line. The hardness of the overlapped areas decreases because they are heated twice and tempered. To avoid this, partial hardening is usually performed by using the moving heat source intermittently. However, the semiconductor laser hardens wide areas. In addition, this problem could be circumvented if we align multiple, and laterally-long heat sources. Therefore, the semiconductor laser could be advantageous as a heat source for surface processing.

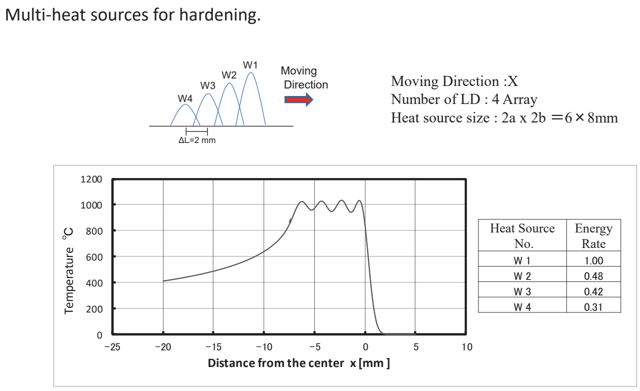

Fig. 14. Technique to equalize the surface temperature using numerical calculation.

5. Processing Experiment with Direct-Processing Semiconductor Laser

5.1. Experiment Equipment Used for Processing

Next, we performed a processing experiment using actual equipment. We used a laser oscillator (DDL) made by Hamamatsu Photonics K.K. and a semiconductor laser-processing machine made by Enshu Limited with an oscillator of maximum power 4 kW. The equipment used in the experiment consisted of stacked LD arrays where 32 LD bars are mounted in parallel to realize the high-power output of DDL. Three or four LD arrays are stacked to synthesize a heat source to obtain several kilo-watts of power.

Usually, the optical system prevents the laser beam from several stacked LDs from broadening. It is extracted as parallel beam by collimation and concentrated by lenses. The laser beam is overlapped and extracted as a single heat source. The semiconductor processing head of the equipment is tilted to radiate an incident beam to a material surface at an angle of several degrees to prevent reflection. **Fig. 15** shows the processing equipment with the semiconductor laser used in the experiment. The processing head integrated with the equipment radiates a laser beam at an incident angle of several degrees from a direction normal to the material to prevent reflection. The influence from the tilted radiation of the heat source is relatively small. However, the authors reported through an experiment that, compared to vertical radiation, laser radiation at a tilt angle of 75° increases the hardened width by 2%–3% and decreases the hardened depth by 3% [3]. Moreover, an assist gas is injected from the side when necessary. The bottom of the heat source is rectangular, but the side face of the heat source when viewed from the y-direction, has a Gaussian-distribution, and therefore the diameter of the Gauss heat source needs to be specified. Here, we used a general spot diameter of $1/e^2$.

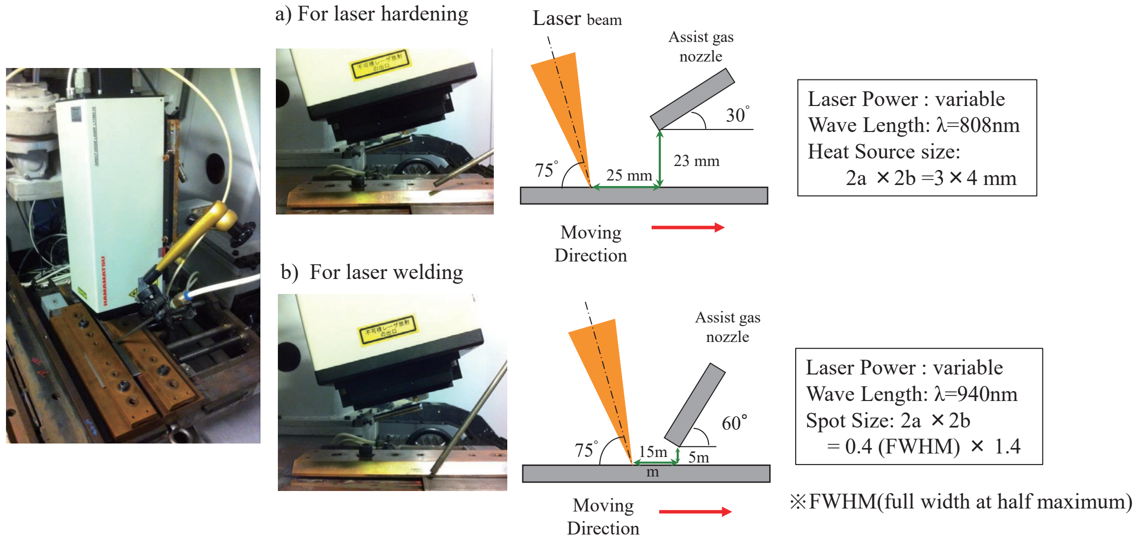

Fig. 15. Experiment set-up of laser processing with DDL.

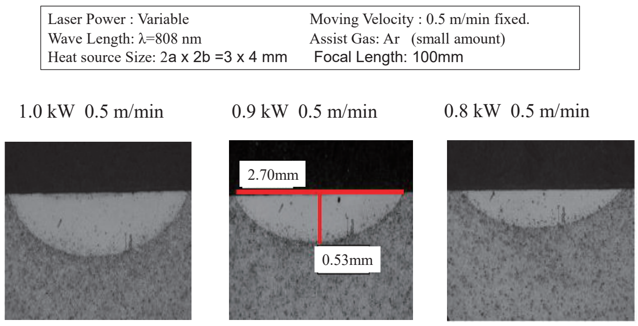

Fig. 16. Experimental results of laser hardening with fixed velocity (0.5 m/min) with DDL.

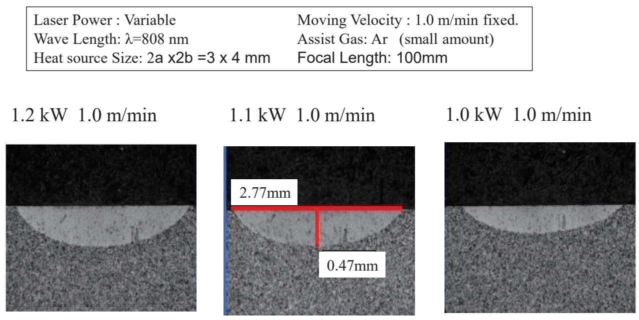

Fig. 17. Experimental results of laser hardening with fixed velocity (1.0 m/min) with DDL.

5.2. Application to Material Processing

5.2.1. Surface Hardening Experiment

We investigated surface hardening with a heat source moving in the lateral direction, i.e., x-direction. A rectangular heat source 3 mm $\times$ 4 mm in size was used for the surface hardening of soft steel. The speed was fixed to 0.5 m/min and the laser power was changed in the range from 0.8 to 1 kW. The oscillation wavelength of the semiconductor laser used for the hardening was $\lambda = 808$ nm.

Figure 16 shows a cross-section of the surface hardening imparted by the equipment. In general, for surface hardening, it is necessary to avoid melting on the surface, but the hardening depth increases with increasing power. **Fig. 17** shows a cross-section of the surface hardened at a constant speed of 1.0 m/min (twice as high as that in the aforementioned experiment) with power changing in the range from 1.0 kW to 1.2 kW. Similarly, an increase in power increases the hardened depth. However, the higher speed decreases the overall hardened depth, that is, a change in the power or the speed affects the cross-sectional shape.

Figure 18 shows a change in the hardened depth (depth

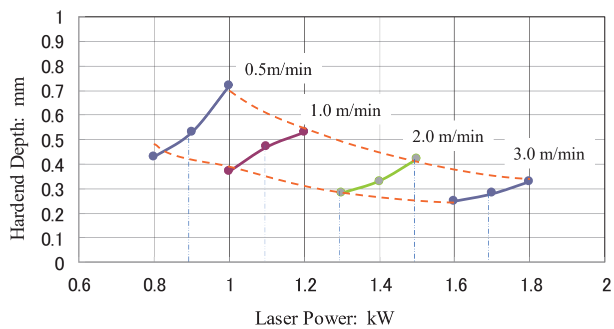

Fig. 18. Experiment results of laser hardening experiment with DDL (single heat source). Effects of hardened depth and laser power as functions of velocity.

of hardened area). Three conditions of power are used for each speed. The hardened depth decreases with increasing speed and increases with the increasing laser power. We compared the hardening imparted by our equipment to that imparted by another laser under identical conditions, ignoring the difference in wavelength. The hardened depth for the DDL processing equipment is 10%–20% larger than that using the CO_2 laser (wavelength of

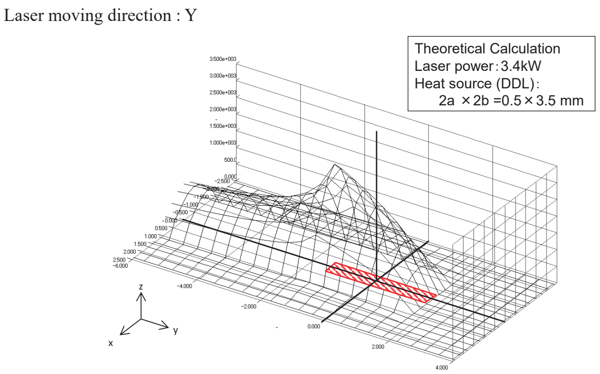

Fig. 19. Temperature distribution of DDL for movement in the lengthwise direction (*y*-direction).

Results of Bead-on-plate experiment

Sample No.	Power 【kW】	Feed Speed 【m/min】	Gas Flow Rate 【L/min】	Gas Blow Angle 【deg.°】	Bead Width 【mm】	Bead Depth 【mm】
1	4	1	20	60	4.083	3.801
2	4	2	20	60	3.356	2.583
3	4	3	20	60	2.815	1.84
4	4	4	20	60	2.366	1.376
5	4	5	20	60	1.825	1.083
6	4	6	20	60	1.516	0.974

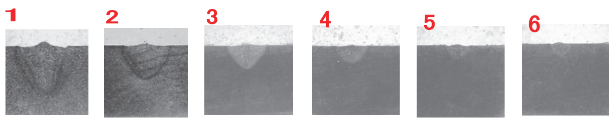

Fig. 20. Experimental results of bead-on-plate on mild steel for movement in the lengthwise direction.

$\lambda = 10{,}600$ nm) under the same condition of power [1, 2]. This could be due to the absorption property of DDL which has a small wavelength.

5.2.2. Surface Melting Experiment

Next, we performed a bead-on-plate experiment where the heat source moved in a single direction on the surface. With this method, one can see the degree of melting and the melting performance (depth, width, and melting shape) of the material surface for different powers and speeds. In other words, this method can be used to study the change in the melting state for different conditions of the laser heat source. This is sometimes called a bead-on-plate welding but it is different from "welding" which melts and joins two or more materials.

Figure 19 shows a typical example of the temperature distribution theoretically calculated for a heat source moving in the *y*-direction (longitudinal direction) for material processing. The peak position of the temperature from this thin heat source lies behind the center, and the temperature distribution has a characteristic long tail.

Figure 20 shows a result of the experiment with a power of 4 kW and speed changing in the range from 1 to 6 m/min. The oscillation wavelength of the semiconductor laser used for the equipment is $\lambda = 940$ nm.

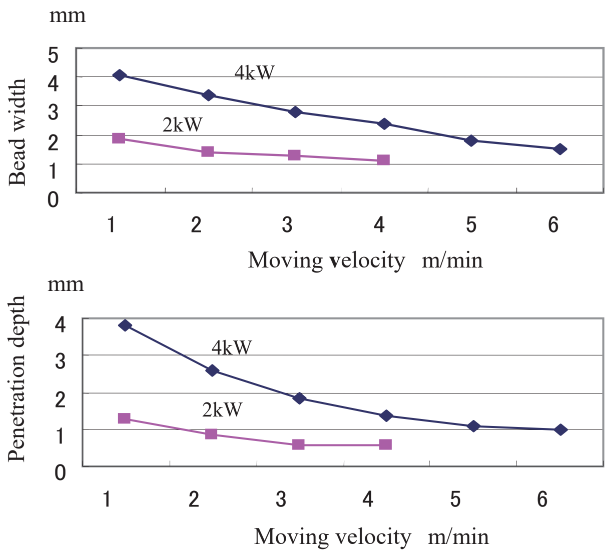

Fig. 21. Effects of power and velocity on melting area by bead-on-plate of the mild steel.

Fig. 21 shows a graph of the bead width and the melting depth measured in the experiment. An increase in the laser power leads to a wider bead and deeper melting.

The conventional shape of the semiconductor laser is rectangular, but laser beams can now be made into a circular spot using beam-shaping technology [14]. The circular heat source was produced for use in cutting. However, the beam-shaping often deforms the intensity distribution. The distribution becomes uniform inside the spot because the extracted laser beams penetrate a process fiber. Therefore, as a result of the uniform energy-intensity distribution inside the spot, one can mathematically regard it as a uniform circular heat source or pseudo-Gaussian distribution heat source. In this case, the calculation is simple and the Gaussian distribution has already been analyzed [2]. Therefore, we omit the analysis and limit ourselves to the DDL heat source.

6. Conclusions

1) For the high-power semiconductor lasers that have been widely used in recent years, we mathematically modeled the laser heat source based on the energy-intensity distribution of the direct-processing semiconductor laser. Then, we derived an analysis theory to calculate the temperature distribution with the heat source moving under given conditions.

2) Using the developed theory, we analyzed the temperature distribution and temperature increase in the material surface processed with semiconductor laser (DDL). As a result, we obtained the temperature distribution specific to the semiconductor laser. We found that DDL processing achieved greater hardened depth and larger melting depth than the known means of hardening, CO_2 laser.

3) In the simulation of applying the direct-processing semiconductor laser, several LDs were aligned in parallel with a constant interval for successive heating in a single direction. To harden the material, the temperature of the material was maintained higher than the transformation point A_1 for a long period by controlling the output power of each LD. This technique improved the characteristics of the hardening. In addition, it realized heat processing that can control the surface temperature.

4) The developed theory is expected to be used for the development of a novel surface processing method. The simulation can be used as a basis to find applications for high-power semiconductor lasers for various processing works.

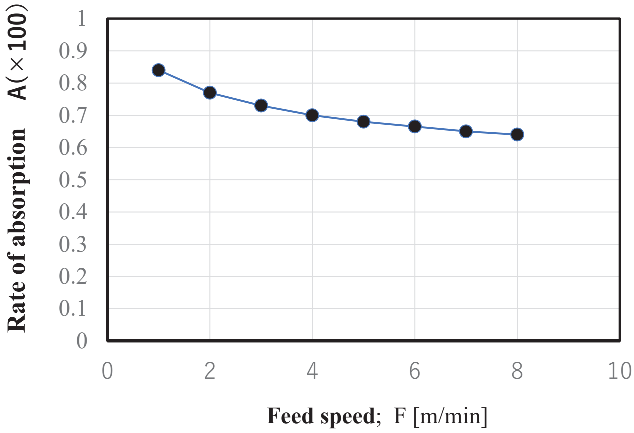

Fig. 22. Absorption rate change with velocity.

References:

[1] H. Kawasumi and T. Arai, "Studies on Surface Hardening wit CO_2 Laser (1st Report) – On the Effects of Rectangular and Modified Rectangular to Laser to Laser Hardening –," J. of Japan Soc. of Prec. Engg., Vol.47, No.6, pp. 669-674, 1981 (in Japanese).

[2] H. Kawasumi and T. Arai, "Studies on Surface Hardening wit CO_2 Laser (2nd Report) – On the Effects of Heart Source Pattern of Gaussian and Doughnut Beam to the Laser Hardening –," J. of Japan Soc. of Prec. Engg., Vol.47, No.12, pp. 1470-1475, 1981 (in Japanese).

[3] H. Kawasumi and T. Arai, "Studies on Surface Hardening wit CO_2 Laser – Effects of Metal Thickness and Irradiation Angle on Characteristics of Laser Hardening –," J. of Japan Soc. of Prec. Engg., Vol.48, No.9, pp. 1238-1243, 1982 (in Japanese).

[4] Y. Arata et al., "Application of Material Processing," I.I.W. Proc., 212-436-78, 1978.

[5] L. Li, "The advances and characteristics of high-power diode laser materials processing," Optics and Lasers in Engineering, Vol.34, Issues 4-6, pp. 231-253, 2000.

[6] L. Qi and Y. Namba, "Precision laser adjustment using CW diode laser," Precision Engineering, Vol.35, No.1, pp. 126-132, 2011.

[7] T. Manzur, A. J. DeMaria, W. Chen, and C. Roychoudhuri, "Potential role of high-power laser diode in manufacturing," Proc. of Photonics West'96, 1996, San Jose, CA, United States, Vol.2703, pp. 490-501, 1996.

[8] F. Bachmann, "Industrial applications of high power diode lasers in materials processing," Applied Surface Science, Vol.208, No.1, pp. 125-136, 2003.

[9] E. Kennedy, G. Byrne, and D. N. Collins, "A review of the use of high power diode lasers in surface hardening," J. of Materials Processing Technology, Vols.155-156, pp. 1855-1860, 2004.

[10] G. Costa Rodrigues, J. Pencinovsky, M. Cuypers, and J. R. Duflou, "Laser cutting with direct diode laser," Optics and Lasers in Engineering, Vol.61, pp. 31-38, 2014.

[11] G. Costa Rodrigues, M. Cuypers, E. Fallahi Sichani, K. Kellens, and J. R. Duflou, "Laser cutting with direct diode laser," Physics Procedia, Vol.41, pp. 558-565, 2013.

[12] S. W. Williams, G. Scott, and N. J. Calder, "Direct Diode Laser Welding of Aerospace Alloys," LaserOpto, Vol.33, No.4, pp. 50-54, 2001.

[13] T. Arai, T. Asano, S. Suzuki, and Y. Harada, "Several Processing with the High Power DDL Laser," Proc. of Japan Soc. of Prec. Engg., 2013 Spring Meeting, pp. 578-580, 2013 (in Japanese).

[14] M. Reyes, K. M. Nowak, F. Villarreal-Saucedo, B. Chann, W. Zhou, and P. Tayebati, "Dynamic Beam Shaper (DBS) for high-power/high-brightness direct diode laser (DDL)," Proc. SPIE 10744, Laser Beam Shaping XVIII, 107440W, 2018.

[15] H. S. Carslaw and J. C. Jaeger, "Heat Conduction in Solid," Oxford University Press., p. 225, 1957.

[16] T. Arai, "High power laser Processing Technology," Machinist Publishing, p. 164, 2004 (in Japanese).

[17] T. Arai, "Metal surface Hardening with CO_2 Laser," Ph.D. thesis, Chuo University, pp. 76-78, 1983.

[18] Y. S. Touloukian et al., "Thermal conductivity: Metallic Elements and Alloys," Plenum Press, 1970.

[19] D. T. Swift-Hook, "Thermophysical Properties," Physics in Technology, Vol.16, No.2, pp. 88-92, 1985.

Appendix A. Rate of Absorption

The laser absorption rate of a laser-processed material changes depending on the moving speed of the laser beam. Therefore, it has speed dependence. The relation is shown in **Fig. 22** where *A* represents the laser absorption rate [16].

Appendix B. Thermal Constants

For theoretical analysis based on heat conduction theory, we need to know the thermal constants (thermal conductivity, thermal diffusivity, and specific heat) of metal. The thermal constants are known to change with the temperature. It has been considered that the exact calculation of the change is difficult because the temperature in laser processing increases rapidly to high temperature. However, this method has been used since the development of the laser flash technique. Graphs of temperature dependence were created with the measurement data of the authors [17] by referring to a large amount of data [18, 19]. The temperature dependences of the thermal constants of typical carbon steel (S45C and SK5) are shown in **Figs. 23–25**.

Figure 23 shows the temperature dependence of the thermal conductivity, **Fig. 24** shows that of the thermal diffusivity, and **Fig. 25** shows that of the specific heat [17, 18].

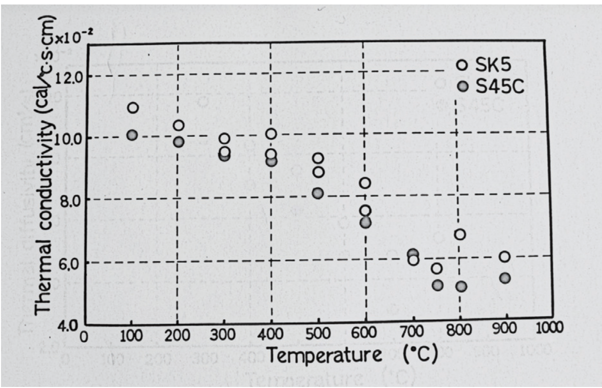

Fig. 23. Temperature dependence of thermal conductivity (for carbon steel).

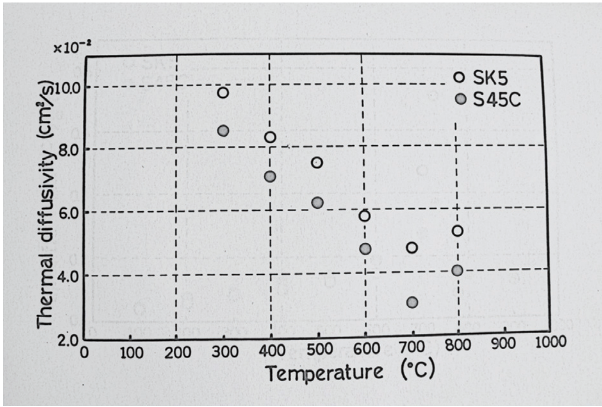

Fig. 24. Temperature dependence of thermal diffusivity (for carbon steel).

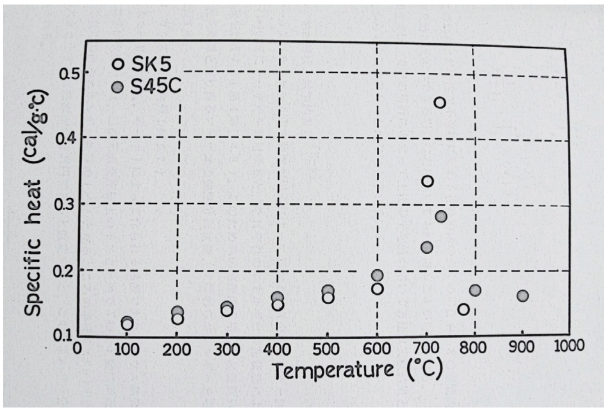

Fig. 25. Temperature dependence of specific heat (for carbon steel).

Name:
Takeji Arai

Affiliation:
Fellow, Research and Development Initiative, Chuo University

Address:
1-13-27 Kasuga, Bunkyo-ku, Tokyo 112-8551, Japan

Brief Biographical History:
1976-1977 Researcher Associate, Tokyo University of Education
1979-1986 Researcher Assistant / Full Time Lecturer, Chuo University
1986-1990 Senior Researcher, Basic Laboratory, FANUC CORPORATION
1990-2001 General Manager, Laboratory for Advanced Laser Technology, Amada Co., Ltd.
2001-2019 Professor, Research and Development Initiative, Chuo University
2019- Fellow, Research and Development Initiative, Chuo University

Main Works:
- "Mechanical Engineering Series, Basic Laser Processing," The Nikkan-Kogyo Shimbun Ltd., 2007.
- "Fundamental Engineering Science for laser Materials Processing," Maruzen Publishing, 2013.
- "Welding and Cutting," The Nikkan-Kogyo Shimbun Ltd., 2014.

Membership in Academic Societies:
- Japan Society for Precision Engineering (JSPE)
- Japan Society of Laser Technology (JSLT)
- Laser Society of Japan (LSJ)